Monatshefte für Chemie 136, 347–366 (2005)
DOI 10.1007/s00706-004-0279-2

Monatshefte für Chemie
Chemical Monthly
Printed in Austria

The Exciton Model and the Circular Dichroism of Polypeptides

Robert W. Woody*

Department of Biochemistry and Molecular Biology, Colorado State University, Fort Collins, CO 80525, USA

Received October 5, 2004; accepted (revised) November 19, 2004
Published online March 8, 2005

Summary. Exciton coupling of the 190 nm $\pi\pi^*$ transition is an important factor in the CD spectrum of peptides and proteins. The CD spectrum of the α-helix is dominated by the exciton effect. The spectrum is sensitive to the direction of the $\pi\pi^*$ transition dipole moment, especially for short helices. Exciton theory is much less successful in accounting for the CD spectrum of the poly(proline)II (*PP*II) conformation, an important conformer in collagen and in unordered peptides. Mixing of the $\pi\pi^*$ transition with high-energy transitions in the peptide backbone and in side chains must be considered to explain the strong negative CD band near 200 nm of *PP*II.

Keywords. Circular dichroism; Helical structures; Peptides; Excitons; Transition moments.

Introduction

The exciton model has had an enormous impact on our theoretical understanding of absorption and circular dichroism (CD) spectra of proteins and nucleic acids, starting with the seminal work of *Moffitt* [1] on helical polypeptides. In a polypeptide, the amide chromophores exhibit little overlap or charge transfer. Thus, to a good approximation, the Hamiltonian for a polypeptide chain with N amides can be taken to be as shown in Eq. (1) where H_i is the Hamiltonian for the group i and V_{ij} represents the *Coulomb* interaction between the electrons and nuclei in groups i and j. The ground-state wave function for the polypeptide is then approximated by the product of the wave functions for the individual amides in their ground state (Eq. (2)).

$$H = \Sigma_i H_i + \Sigma_i \Sigma_{j>i} V_{ij} \tag{1}$$

$$\Psi_0 = \varphi_{10} \cdots \varphi_{N0} \tag{2}$$

Excited states can be described by a linear combination of wave functions in which one, two, ..., amide groups are excited. In keeping with the normal exciton

* E-mail: robert.woody@colostate.edu

approximations, we will confine ourselves to configurations in which a single amide is excited (Eq. (3)) where $\Psi_{j\mathrm{a}} = \varphi_{10} \cdots \varphi_{j\mathrm{a}} \cdots \varphi_{\mathrm{N}0}$ is the wave function for the configuration in which amide j is in excited state a and all other amides are in their ground states. The coefficients $\mathrm{C}_{j\mathrm{aK}}$ describe the delocalization of the excitation over the whole molecule. Given these exciton coefficients, the optical properties of the polypeptide can be calculated. The electric dipole transition moment is described by Eq. (4) where $\boldsymbol{\mu}_{j\mathrm{oa}}$ is the electric dipole transition moment for the transition $0 \rightarrow$a in group j. The magnetic dipole transition moment is given by Eq. (5) where $\mathbf{m}_{j\mathrm{ao}}$ is the magnetic dipole transition moment for the transition $0 \rightarrow a$ in group j.

$$\Psi_{\mathrm{aK}} = \Sigma_j \mathrm{C}_{j\mathrm{aK}} \Psi_{j\mathrm{a}} \tag{3}$$

$$\boldsymbol{\mu}_{0\mathrm{aK}} = (\Psi_0 | \boldsymbol{\mu} | \Psi_{\mathrm{aK}}) = \Sigma_j \mathrm{C}_{j\mathrm{aK}} \boldsymbol{\mu}_{j\mathrm{oa}} \tag{4}$$

$$\mathbf{m}_{\mathrm{a0K}} = (\Psi_{\mathrm{aK}} | \mathbf{m} | \Psi_0) = \Sigma_j \mathrm{C}_{j\mathrm{aK}} \mathbf{m}_{j\mathrm{ao}} \tag{5}$$

In a general polypeptide with no symmetry, transitions to all N excited states have non-zero $\boldsymbol{\mu}_{0a\mathrm{K}}$ and $\mathbf{m}_{a0\mathrm{K}}$ and will be observable in both absorption and CD, but only a few will be resolvable. However, in a helical polypeptide, the symmetry of the helix leads to selection rules. *Moffitt* [1] considered an infinite helix, analogous to a one-dimensional crystal. He assumed periodic boundary conditions, leading to the requirement that the $\mathrm{C}_{j\mathrm{aK}}$ be periodic functions of j and K (Eqs. (6)–(8)).

For $\mathrm{K} = 0$,

$$\mathrm{C}_{j\mathrm{aK}} = \mathrm{N}^{-1/2} \tag{6}$$

and for $\mathrm{K} \neq 0$,

$$\mathrm{C}_{j\mathrm{aK}} = (2/\mathrm{N})^{1/2} \cos(2\pi j \mathrm{K}/\mathrm{N}) \tag{7}$$

and

$$\mathrm{C}_{j\mathrm{aK}} = (2/\mathrm{N})^{1/2} \sin(2\pi j \mathrm{K}/\mathrm{N}) \tag{8}$$

The $\mathrm{K} = 0$ level is non-degenerate, whereas the wave functions (7) and (8) are degenerate.

It is a remarkable fact that of the N exciton levels in an infinite helix, only *three* give rise to non-vanishing transition dipole moments from the ground state. The $\mathrm{K} = 0$ level is one of these. In this case, the coefficients for all residues are identical, and the transition dipoles for all residues in Eq. (4) are additive. This leads to a large resultant along the helix axis, but the perpendicular components cancel. This gives rise to the *parallel exciton band.*

The other way to avoid wholesale cancellation of the transition moments is to insure that the resultant of the transition moments in each turn of the helix is non-zero and that this resultant is the same for every turn of the helix. This requires that $\mathrm{K} = \pm \mathrm{N}/\mathrm{P} = \pm \mathrm{M}$ the (integral) number of turns in the helix. The two degenerate exciton levels corresponding to Eqs. (7) and (8) with $\mathrm{K} = \pm \mathrm{N}/\mathrm{P}$ give rise to resultants in each turn of the helix that are perpendicular to the helix, and the large resultants for the whole helix are orthogonal to each other. These bands are called the *perpendicular exciton bands.*

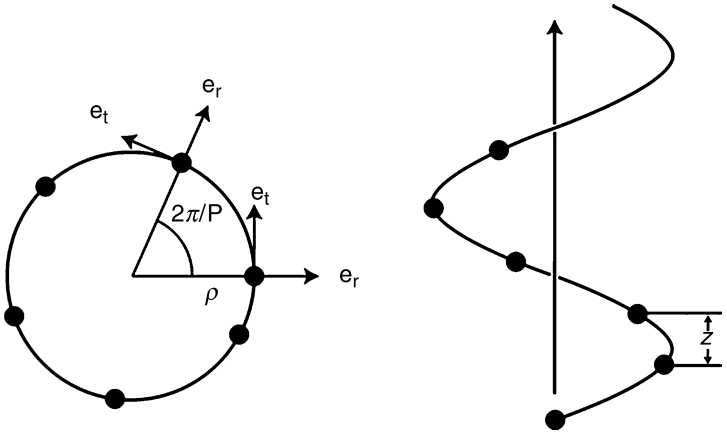

Fig. 1. Geometry of a helix; the axial translation *per* residue is z and the angular displacement per residue is $2\pi/\mathrm{P}$, where P is the number of residues per turn; the local coordinate systems at two successive transition centers at radius ρ are shown; the right-handed coordinate system used to define the orientation of the electric dipole transition moments in Eqs. (11)–(14) is formed by the vectors $\mathbf{e}_r$, $\mathbf{e}_t$, and $\mathbf{e}_v$, the latter of which is directed toward the viewer

The frequencies, dipole strengths, and rotational strengths from the *Moffitt* bands are as follows in Eqs. (9)–(14) where ν_0 is the frequency (cm^{-1}) of the transition in the monomer; $\nu_{||}$ and $\nu_\perp$ are the frequencies of the parallel and perpendicular *Moffitt* bands; V_{0j} is the *Coulomb* interaction between the transition density for 0→a in group j and that at the level 0; P is the number of residues per turn; $D_{||}$ and $D_\perp$ are the dipole strengths for the parallel and perpendicular exciton bands; $R_{||}$ and $R_\perp$ are the corresponding rotational strengths; μ_r, μ_t, μ_v are the transition moment components radial, tangential, and vertical to the helix, which form a right-handed coordinate system as illustrated in Fig. 1; and ρ is the distance of the chromophore center from the helix axis (Fig. 1).

$$\nu_{||} = \nu_0 + (2/hc)\Sigma_j V_{0j} \tag{9}$$

$$\nu_\perp = \nu_0 + (2/hc)\Sigma_j V_{0j} \cos 2\pi j/\mathrm{P} \tag{10}$$

$$D_{||} = {\mu_v}^2 \tag{11}$$

$$D_\perp = ({\mu_r}^2 + {\mu_t}^2)/2 \tag{12}$$

$$R_{||} = \pi\rho\nu_{||}\mu_v\mu_t \tag{13}$$

$$R_\perp = -\pi\rho\nu_\perp\mu_v\mu_t \tag{14}$$

To visualize the nature of the exciton wave functions, energies, transition moments, and rotational strengths, it is helpful to consider a helix with four amide groups per turn, as *Moffitt* [2] did. Such a helix is similar to the α-helix with 3.6 residues/turn, but the integral value of P makes visualization simpler. Figure 2a illustrates the parallel exciton components for a right-handed helix with $\mathrm{P} = 4$. The four transition moments in one turn of the helix are all in phase, their perpendicular

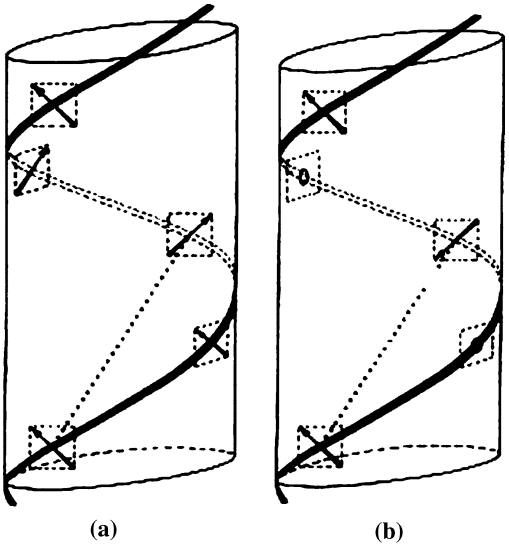

Fig. 2. Exciton states in a polypeptide helix with P = 4; (a) parallel exciton band; (b) one of the perpendicular exciton bands (from Ref. [2])

components cancel, and their parallel (vertical) components reinforce. Notice also that the transition moments interact predominantly in a head-to-tail fashion, corresponding to electrostatic attraction, *i.e.*, the interactions decrease the transition energy relative to that of the isolated chromophore. Thus the parallel band is red-shifted in this model helix. To determine the direction of the magnetic dipole transition moment, required for predicting CD, we must consider the circulation of charge in the transition. We can visualize the circulation of charge by connecting the head on one transition moment vector with the tail of the next. We then curl the fingers of our right hand in the direction of this circulation. The right thumb then points in the direction of the magnetic dipole transition moment. By this right-hand rule, the magnetic dipole transition moment for the K = 0 band is directed downward, opposite in direction to the electric dipole transition moment. Therefore, the parallel exciton band is predicted to give rise to a negative rotational strength.

Figure 2b refers to one of the perpendicular exciton components. Here, the exciton coefficients are $+1$ for the amide at the bottom of the helix, -1 for the amide at the back, and 0 for the amides on the right and left. The vertical components cancel and the two non-zero transition moments add to give a transition moment for one turn that is directed to the left. The non-zero transition moments on opposite sides of the helix interact in a predominantly head-to-head and tail-to-tail fashion. Therefore, the perpendicular exciton band is predicted to be blue-shifted relative to the isolated monomer transition. The circulation of charge is clockwise as seen from the right of the helix, giving rise to a magnetic dipole transition moment that is directed to the left of the helix, parallel to the electric dipole transition moment. The rotational strength of the perpendicular band is therefore predicted to be positive by this heuristic model. The other perpendicular component is obtained by assigning coefficients of 0, $+1$, 0, and -1 reading from bottom to top of the helix.

Quantitative application of *Moffitt*'s theory to the α-helix [2], using the geometry of *Pauling et al.* [3] and the amide $\pi\pi^*$ transition moment direction from

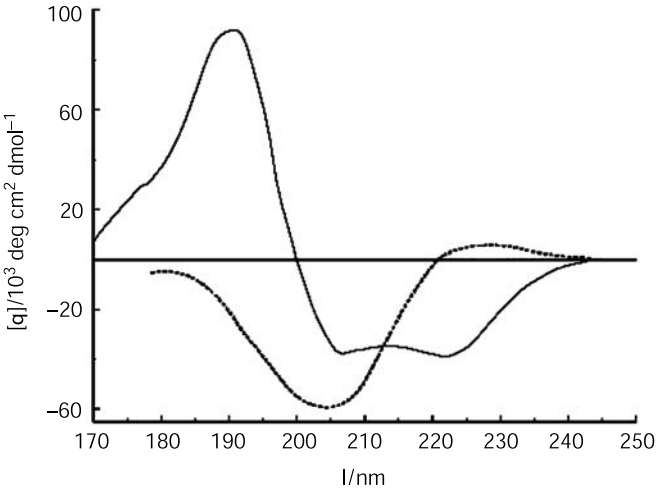

Fig. 3. CD spectra of polypeptides in the α-helix (———) [13] and poly(*Pro*)II (------) [14] conformations

myristamide crystals [4, 5], led to the prediction of an exciton splitting of $\nu_{||} - \nu_{\perp} = -2800\,\mathrm{cm}^{-1}$, with the parallel band having a negative rotational strength for a right-handed helix, *i.e.*, a negative exciton couplet was predicted for this helix sense. Although there were no absorption or CD data available for α-helical polypeptides at the time, the predicted negative exciton couplet was shown to be consistent with optical rotary dispersion data for helical polypeptides, accounting for a qualitative difference in ORD behavior between helical and unordered polypeptides [6]. Further confirmation of *Moffitt*'s theory came five years later with the observation of a shoulder at ~205 nm on the main 190-nm absorption band in α-helical polypeptides that was absent in unordered polypeptides [7, 8]. Linear dichroism measurements of films [9] and solutions [10] supported the polarization predictions for the 205- and 190-nm bands. The first CD measurements for the α-helix [11, 12] confirmed that the right-handed α-helix has a negative CD band near 205 nm and a positive band near 190 nm, as shown in Fig. 3. The 222-nm negative band is assigned as the amide $n\pi^*$ transition.

The Helix Band

A significant contribution to the CD spectrum of helical polypeptides was lacking in *Moffitt*'s theory, however, as realized upon comparison with a theoretical formulation in which periodic boundary conditions were not assumed [15]. Subsequent studies [16–18] have shown that the term was missed because the periodic boundary conditions used by *Moffitt* [1] are incompatible with the *Rosenfeld* [19] formulation of the rotational strength. Periodic boundary conditions require dimensions that are large compared with the wavelength of light whereas the *Rosenfeld* formulation requires dimensions much less than the wavelength. The *Moffitt* bands arise from light propagating perpendicular to the helix axis, in which case the helix dimensions are small compared to the wavelength and the *Rosenfeld* formulation is valid. However, *Moffitt*'s theory predicts zero CD for light propagating along the

helix axis, a case in which *Moffitt*'s two assumptions are contradictory. In this case, periodic boundary conditions can be applied, but the dipole approximation leading to *Rosenfeld*'s expression for the rotational strength must be avoided.

Consideration of retardation effects leads to a modification of the selection rules for light propagating along the helix axis [16–18]. The allowed transitions are to exciton levels $K = N\ (\pm P^{-1} + z/\lambda)$ rather than $N\ (\pm P^{-1})$, where z is the axial translation per residue (Fig. 1) and λ is the wavelength of the transition in the monomer. For the α-helix, $z/\lambda \cong 0.15/200 \sim 10^{-3}$, whereas $P^{-1} = (3.6)^{-1} = 0.28$. Therefore, the degeneracy of the perpendicularly polarized exciton levels is broken, but the two allowed levels are still nearly degenerate. However, the rotational strengths of these two levels are huge and are of opposite sign. For $K = \pm N/P$, as we have seen, the electric dipole transition moment for each turn of the helix is perpendicular to the helix axis and constant in direction as one moves along the helix. The modified selection rules lead to modes in which the resultant electric vector rotates slowly about the helix axis from one turn to the next, executing one full turn over one wavelength of the light. This means that for one of these exciton modes, the local electric dipole transition moment is always in phase with the electric vector of one form of circularly polarized light, *e.g.*, right-circularly polarized light (rcp). Therefore, transitions to this level will absorb rcp strongly, but will not absorb lcp at all, *i.e.*, they will exhibit perfect CD and have a huge negative CD. The other mode will exhibit perfect CD for lcp, have a correspondingly enormous positive CD. The rotational strengths grow without bound as N increases, but the energy separation decreases with increasing N, giving rise to a finite couplet in CD. *Tinoco* [20] showed that, for *Gaussian* band shapes, the CD due to this so-called helix band is given by Eq. (15) where K is defined by Eq. (16) and Δ is half the width of the *Gaussian* band at e^{-1} of its maximum.[a]

$$[\theta]_h = K[2(\lambda_\perp - \lambda)\lambda_\perp/\Delta^2 + 1]\exp\left[-(\lambda - \lambda_\perp)^2/\Delta^2\right] \tag{15}$$

$$K = -(48\pi^{5/2} N_0\, z\, \lambda_\perp {\mu_\perp}^2/h^2c^2\Delta)\, \Sigma_j V_{0j} \sin(2\pi \boldsymbol{j}/P) \tag{16}$$

The existence of this helix band has been controversial. *Mason* [21] argued that the additional contribution is an end effect that should be of minimal importance for long helices. However, *Holzwarth* and *Doty* [22] refuted *Mason*'s arguments. Calculations on the α-helix [23] showed that the helix term gives a strong positive couplet, and the negative lobe of this couplet was predicted to give rise to negative CD on the short-wavelength side of the positive 190-nm band. ORD [24] and CD [25] measurements showed that the CD spectrum of the α-helix has a positive shoulder near 175 nm rather than a negative band (Fig. 3). A careful analysis of the isotropic absorption and CD spectrum of the α-helix, combined with linear dichroism and oriented CD measurements [10], provided experimental evidence for the helix band, although it was found to be weaker than predicted by a factor of about four. The present work provides an explanation for this discrepancy.

[a] Due to a misprint, the minus sign in Eq. (16) was missing in *Tinoco*'s 1964 paper [20]. Comparison with the expression for ORD derived by *Moffitt et al.* [13] shows that the minus sign should be there. *Woody* and *Tinoco* [23] used the correct form of Eq. (16)

Results and Discussion

Excitons in Finite α-Helices

The exciton model was applied by *Tinoco* and coworkers [26] to finite α-helices. The coefficients in the exciton wave function (Eq. (1)) were obtained by diagonalizing the Hamiltonian matrix (Eq. (17)).

$$\begin{pmatrix} E_0 & V_{01} & V_{02} & V_{03}\cdots \\ V_{01} & E_0 & V_{01} & V_{02}\cdots \\ V_{02} & V_{01} & E_0 & V_{01}\cdots \\ \cdots & & & \end{pmatrix} \tag{17}$$

The E_K are obtained as the eigenvalues of the matrix and the C_{iaK} as the eigenvectors. Figure 4a shows the rotational strengths for α-helices of increasing chain lengths calculated using *Peterson* and *Simpson*'s transition moment direction [5]. Even for relatively short helices, only a few exciton levels have significant dipole strengths (not shown) and rotational strengths. The exciton levels with predominantly parallel polarization in absorption are indicated in the figure. The remaining

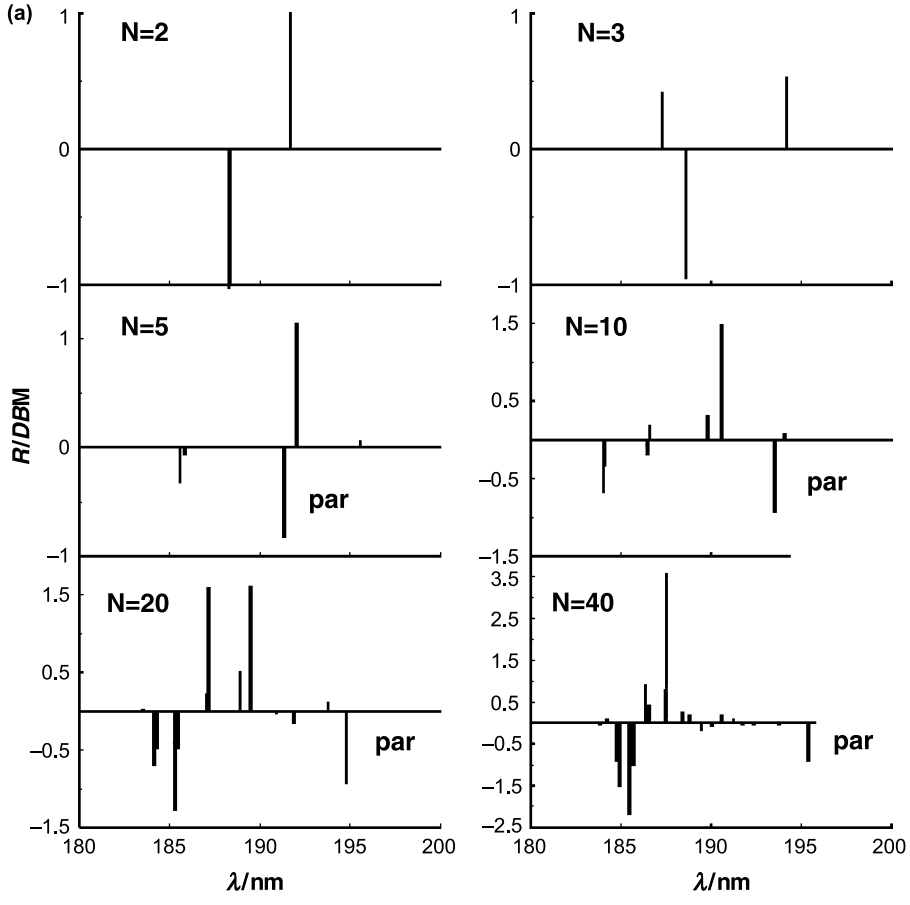

Fig. 4 (*continued*)

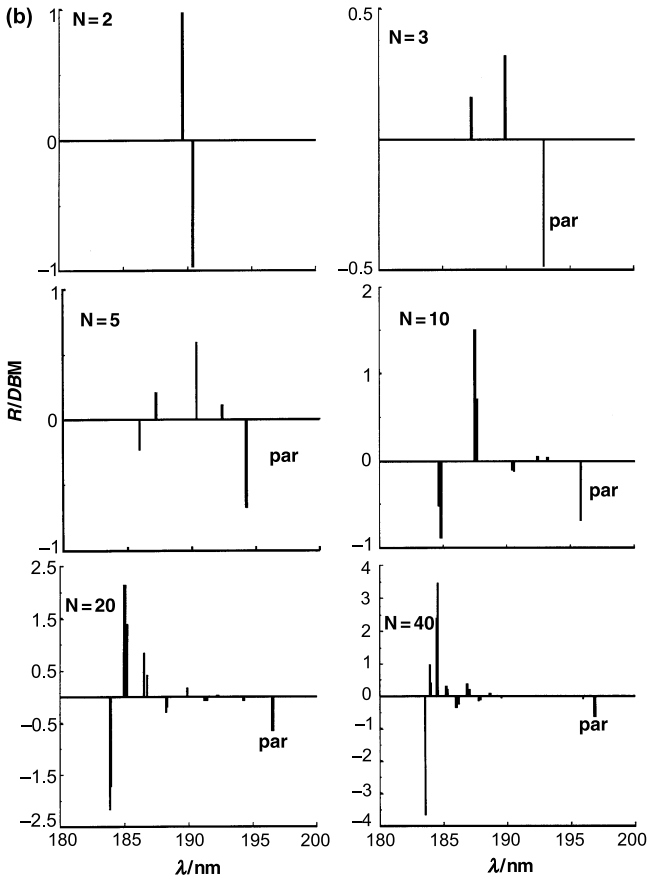

Fig. 4. Rotational strengths for the NV_1 exciton levels of finite α-helices as a function of N, the helix length, and θ, the transition moment direction; these calculations considered only the NV_1 transition; the transitions marked *par* are predominantly polarized along the helix axis; unmarked transitions are predominantly polarized perpendicular to the helix axis; note the differences in vertical scale for different helix lengths; (a) $\theta = -41°$ [5]; (b) $\theta = -55°$ [28]

levels have predominantly perpendicular polarization. It can be seen that the polarization of the exciton levels is relatively pure even for short helices.

A single parallel-polarized exciton level is observed on the long-wavelength edge of the NV_1 exciton band for all helices with $N > 8$. This band has a strong negative rotational strength that does not increase markedly with chain length. This band in finite helices corresponds to the parallel-polarized *Moffitt* band in the infinite helix.

At shorter wavelengths, the exciton levels in finite helices are more complex and are largely of perpendicular polarization. It is clear that the rotational strengths are predominantly positive above $\sim$186 nm and predominantly negative below that wavelength. As the helix length increases, these perpendicularly polarized transitions tend to cluster more tightly, and the CD intensities of the strongest transitions increase. If we assign finite widths to the corresponding CD bands, these bands give rise to a single positive band and a symmetrical couplet that is positive on the long-wavelength side and negative on the short-wavelength side. The single

positive band corresponds to the perpendicular-polarized *Moffitt* band in the infinite helix, and the couplet corresponds to the helix band.

The mixing of different electronic transitions is now treated almost exclusively by the matrix method, developed by *Schellman* and coworkers [27] and described in the methods section. This is a generalization of the exciton method that can treat the mixing of the NV_1 transition with the peptide $n\pi^*$ and NV_2 transitions, as well as with side-chain transitions in aromatic side chains. In the following, we shall use the term *exciton contributions* in the generalized sense of the results of mixing of discrete transitions as obtained by the matrix method and not limit it to the restricted sense of mixing of degenerate excited states.

Effect of Transition Moment Direction

The amide NV_1 transition moment direction for myristamide [5] was used by *Moffitt* [2] in his calculation and in many subsequent calculations. However, myristamide is a primary amide, whereas the peptide group is a secondary amide, except for *X-Pro* peptides that are tertiary amides. No definitive determination of the transition moment direction for a secondary amide was reported until *Clark*'s study of *N*-acetylglycine [28]. *Clark* found that, whereas primary amides have the NV_1 transition polarized at an angle of $\sim -40^\circ$ with respect to the carbonyl bond direction, the transition is polarized at $\sim -55^\circ$ in the secondary amide *N*-acetylglycine (in this convention, the CN bond lies at a positive angle). Thus, the transition moment directions differ by $\sim$15–20° for the two types of amides.

Although 15° does not seem like a large difference, the exciton CD depends quite strongly on the NV_1 transition moment direction. Figure 5 shows CD spectra

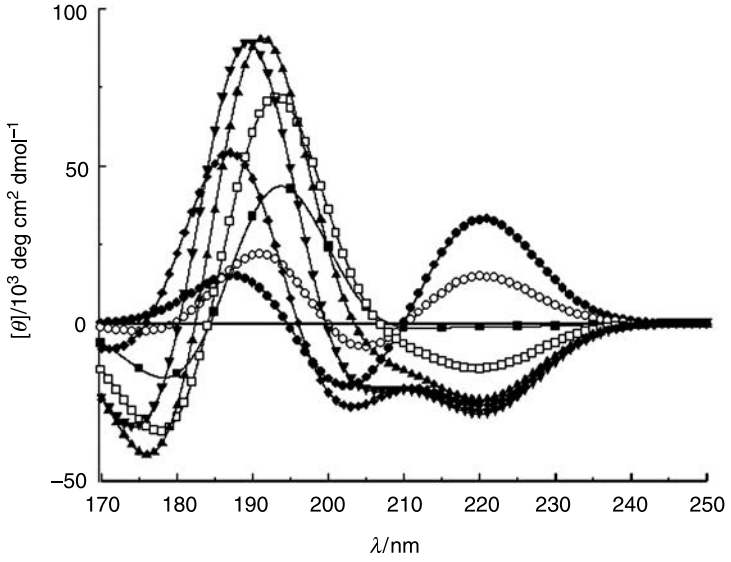

Fig. 5. CD spectra calculated for an α-helix with $N = 20$ as a function of θ, the NV_1 transition moment direction; note that these calculations used the matrix method and include the mixing of the NV_1 transition with the $n\pi^*$ and NV_2 transitions; $\theta = 0^\circ$, ●; $\theta = -10^\circ$, ○; $\theta = -20^\circ$, ■; $\theta = -30^\circ$, □; $\theta = -40^\circ$, ▲; $\theta = -50^\circ$, ▼; $\theta = -60^\circ$, ◆

calculated for the α-helix using transition moment directions ranging from 0° (parallel to the carbonyl bond direction) to −60° at 10° intervals. The exciton CD in the NV_1 region, neglecting the $n\pi^*$ CD band near 220 nm, varies from a weak negative couplet for $\theta = 0°$ through a three-band spectrum dominated by strong positive or negative couplets, to a strong negative couplet. For the most likely values of θ (−40° and −50°), the exciton CD has a negative band near 205 nm, corresponding to *Moffitt*'s parallel band, and a positive couplet with a positive lobe near 190 nm and a negative lobe near 175 nm. This latter feature results from the combination of *Moffitt*'s perpendicular exciton band and the helix band.

The NV_1 transition moment direction is especially important for the exciton CD of short α-helices. Calculations of the CD spectra of short α-helices [26, 29] using *Peterson* and *Simpson*'s [5] transition moment direction (−41°) predicted that such α-helices should have qualitatively different CD spectra from long helices. It was predicted that the characteristic negative 205 nm band should not be observable for helices with fewer than 10–15 amide groups. For shorter helices, the exciton splitting is insufficient to place the negative *Moffitt* band on the long-wavelength edge of the band or to resolve it from the other exciton levels, as can be seen in Fig. 4a. This prediction was at odds with the observation of α-helical patterns in the CD spectra of globular proteins with distinct negative 205 nm bands, despite average helical segment lengths of ∼10 amides.

Experimental data on short model α-helical peptides of defined length were unavailable until recently, when helices with as few as four amides were shown to be stable in La^{3+} complexes of a peptide from a Ca^{2+}-binding loop of calmodulin [30]. Figure 6 shows the CD spectra [31] for α-helices with 4, 8, and 11 amide groups, all having the characteristic α-helix CD pattern. When the NV_1 transition moment direction for primary amides (−40°) [5] is used to calculate the CD

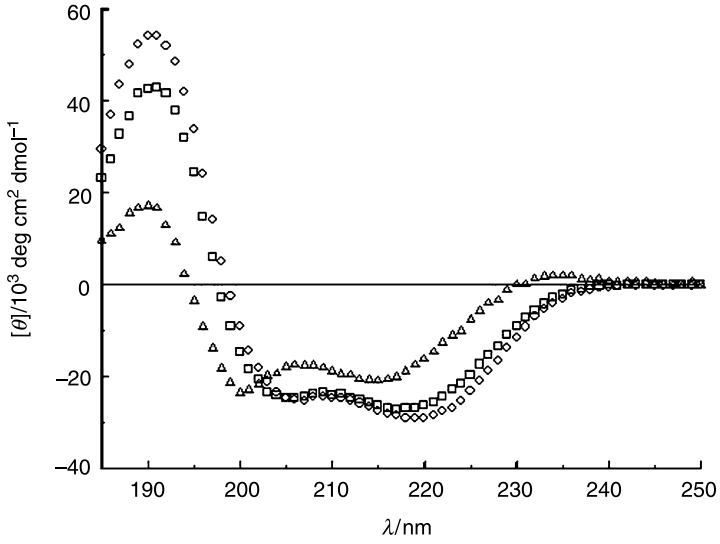

Fig. 6. Experimental CD spectra of α-helices with 4 (△), 8 (□), and 11 (◇) amides [31]; based upon difference spectra of peptides containing a Ca^{2+}-binding loop from calmodulin in the presence and absence of La^{3+}

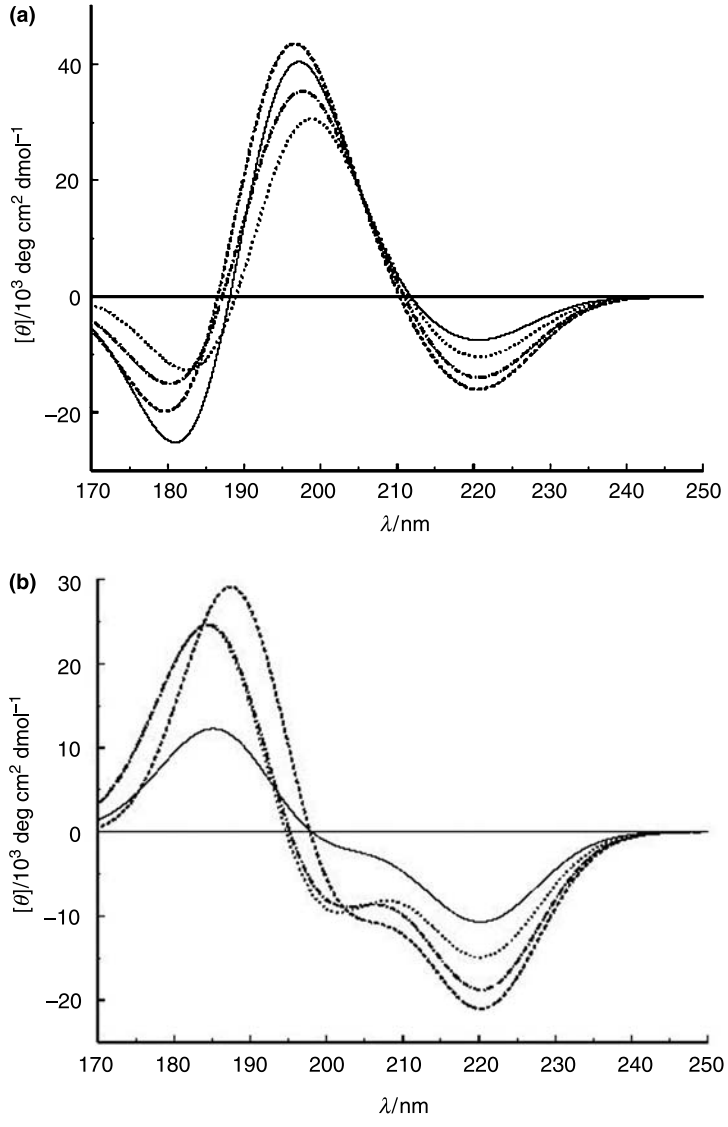

Fig. 7. CD spectra for short α-helices predicted with two different NV_1 transition moment directions; (a) $\theta = -40°$, (b) $\theta = -55°$; dimer (———); trimer (· · · · ·); tetramer (- · · - · ·); pentamer (- - - - - -)

spectra (Fig. 7a), no negative 205 nm band is predicted until helices much longer than 11 amides are considered. Figure 5 shows the spectrum calculated for a helix with 20-amides and $\theta = -40°$, which shows only a negative shoulder near 205 nm. If the NV_1 transition moment direction for secondary amides ($-55°$) [28] is used instead of that for primary amides, the exciton splitting is larger, leading to predicted spectra (Fig. 7b) that show a negative 205 nm band even with four amides. The reason that this 15° rotation has such a dramatic effect is that the nearest-neighbor interaction energy for the NV_1 transition, V_{01}, is opposite in sign for the two directions. For $\theta = -40°$, V_{01} is positive whereas V_{02}, V_{03} *etc.* are negative. Thus, the nearest-neighbor interaction blue shifts the parallel-polarized exciton band (Eq. (9)) but is overcome in longer helices by the negative interaction

energies with more distant neighbors. For $\theta = -55°$, V_{01} is negative as are the interaction energies with more distant neighbors. Therefore, the exciton splitting is larger for all helix lengths, and sufficient to yield an observable negative 205 nm band even for short helices. This is illustrated in Fig. 4b, which shows the rotational strengths for the exciton levels for helices of varying length. Note that with $\theta = -55°$ a negative NV_1 couplet is predicted at the dimer level, in contrast to the positive couplet for $\theta = -40°$ (Fig. 4a). Thus, even for the shortest helix lengths, a negative NV_1 couplet is predicted for $\theta = -55°$.

Excitons in Poly(Pro)II

Poly(*Pro*) can adopt two quite different helical conformations: a right-handed helix with all-*cis* amides that is stable in relatively nonpolar solvents such as higher alcohols, called poly(*Pro*)I; and a left-handed all-*trans* helix that is the stable form in water and trifluoroethanol, called poly(*Pro*)II. Poly(*Pro*)II (*PP*II) is of much wider interest for several reasons. The conformation of *PP*II is nearly identical to that of each of the three individual chains in collagen, an abundant protein of great medical significance. The *PP*II conformation does not require the presence of *Pro* and is observed in segments of proteins lacking *Pro* [32–34]. In fact, *PP*II appears to be the most stable conformation for many peptides in aqueous solution and is an important component of unfolded proteins [35–37].

The CD spectrum of poly(*Pro*)II is shown in Fig. 3. A weak positive band near 225 nm and a strong negative band near 206 nm are observed. These features are also observed in CD spectra of peptides lacking *Pro* but having a substantial *PP*II content [35–37], but the band positions are shifted to shorter wavelengths by ~10 nm. In addition to the strong negative band near 200 nm, the most distinctive feature of the *PP*II CD spectrum is the absence of any positive feature at wavelengths in the NV_1 region and below, down to at least 160 nm [14].

The exciton model was applied to *PP*II by *Mandel* and *Holzwarth* [38] in an analysis of the experimental absorption, CD, LD, and oriented CD spectra of collagen and *PP*II. They reported that the *Moffitt* bands form a positive couplet with the long-wavelength parallel-polarized band positive and the short-wavelength perpendicular band negative. The couplet was biased toward negative values with the perpendicular band 1.5–2-fold more intense. The helix band was found to be a negative couplet.

Using the standard *PP*II geometry from fiber diffraction [39] and the *Peterson* and *Simpson* [5] NV_1 transition moment direction, *Pysh* [40] predicted relatively weak *Moffitt* bands: a positive, red-shifted parallel band and a negative, blue-shifted perpendicular band. The helix band was calculated to be strong and with a negative lobe on the long-wavelength side. The negative lobe of the helix band, combined with the negative perpendicular *Moffitt* band, gave rise to a strong negative band at about 205 nm, which agreed qualitatively with the observed negative band of PPII at 206 nm. However, *Pysh* used *Tinoco*'s [20] equation for the helix band as printed, without the minus sign. Subsequent studies showed that the helix band from the exciton model is predicted to be positive for the standard *PP*II helix geometry. *Ronish* and *Krimm* [41] also reported satisfactory results for calculations on *PP*II, but they included non-exciton contributions and

partially suppressed the exciton bands by assigning larger bandwidths to them, relative to the non-exciton contributions. *Madison* and *Schellman* [29], *Tterlikkis et al.* [42] and *Manning* and *Woody* [43] predicted a strong positive couplet for conformations near the standard *PP*II conformation, contrary to the strong negative band observed. They were able to obtain negative CD near 200 nm only if they modified the *Ramachandran* angles and/or transition moment direction.

Although reasonable agreement near 200 nm can be obtained with conformations deviating from the canonical *PP*II, such calculations all predict sizeable positive bands at shorter wavelengths. Experimentally, no such positive features are observed in the *PP*II CD spectrum down to 160 nm [14]. This reflects an inherent limitation of the exciton model for explaining a spectrum such as that of *PP*II that is uniformly negative over a broad wavelength region. The sum rule for rotational strengths [44] requires that the integral of the CD spectrum over all wavelengths must vanish. The exciton model is consistent with this. The two *Moffitt* bands (Eqs. (13) and (14)) have opposite signs, differing only slightly in magnitude, and the integral over the helix band (Eq. (15)) is nearly zero. Thus, if we only consider the NV_1 transition, the exciton model must give positive and negative CD bands of equal magnitude. Such a CD spectrum is called *conservative*.

The CD spectrum of *PP*II is distinctively *non-conservative*. This implies that the NV_1 transition must mix with electronic transitions at higher energy. The only discrete, well-characterized electronic transition in the amide at higher energies than the NV_1 transition is the second $\pi\pi^*$ (NV_2) transition at about 140 nm [28]. This transition was considered by *Tterlikkis et al.* [42] and by *Manning* and *Woody* [43], albeit without the benefit of *Clark*'s data [28], but mixing of the NV_1 and NV_2 transitions did not resolve the problem in the NV_1 region. The results of matrix method [27] calculations in the present study show that mixing of the NV_1 and NV_2 transitions, the only electrically allowed amide transitions that have been characterized, does not lead to satisfactory agreement with experiment for the *PP*II helix, even if conformations deviating from that derived from fiber diffraction [39] are considered (Fig. 8a and b, dashed curves).

The matrix method [27] can only treat the mixing of discrete, well-characterized transitions amongst themselves. In the case of amides, the matrix method is thus restricted to describing the mixing of the $n\pi^*$, NV_1, and NV_2 transitions. There are, of course, many higher energy transitions in the amide group, the $C_\alpha H$ group of the peptide backbone, and the amino acid side chains. These transitions have not been resolved or characterized. However, their total oscillator strength greatly exceeds that of the known discrete transitions, and they dominate the polarizability.

The contributions to the rotational strengths of each exciton level from the high-energy transitions, $R_{K\alpha}$ from Eq. (23) (Methods), are combined with those from the matrix method obtained by diagonalizing the matrix in Eq. (18) (Methods) to yield the total rotational strength for each K level, and these are used to calculate the CD spectrum. Figure 8a shows the calculated CD spectrum for a standard *PP*II helix with $\theta = -55°$. The polarizable group contribution provides a strong negative couplet centered near 190 nm that enhances the weak negative band near 207 nm in the exciton contribution and largely cancels the positive limb of the exciton couplet centered near 183 nm, creating a negative band in the total

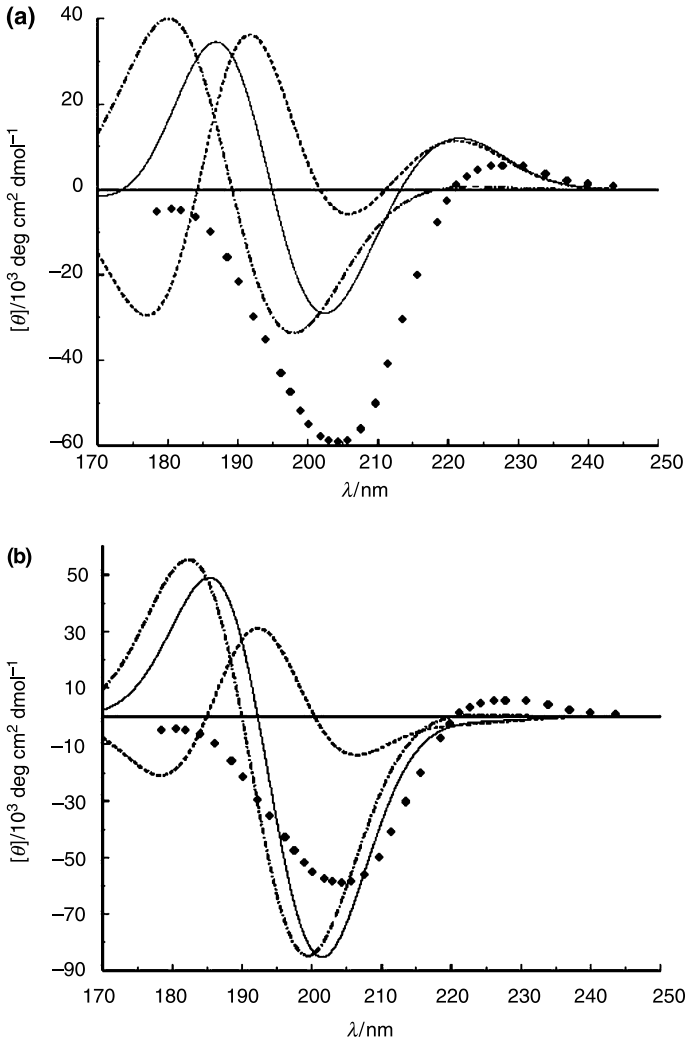

Fig. 8. CD spectra of *PP*II helices with N = 20 calculated using $\theta = -55°$; exciton contribution (- - - - - -); polarizable group contribution (- · - · - · -); total (———); (a) standard *PP*II helix ($-77.2°$, $+145.9°$); (b) non-standard *PP*II helix ($-60°$, $+180°$); The solid circles represent the experimental CD spectrum of *PP*II in water; it should be noted that tertiary amides such as those formed by *Pro* have their $n\pi^*$ and $\pi\pi^*$ absorption and CD bands shifted by ~10 nm to the red relative to secondary amides for which the calculations were performed

CD near 203 nm. However, the negative couplet from polarizable group contributions is nearly symmetrical and the overlap of its positive lobe with the negative short-wavelength lobe of the exciton helix band creates a positive band in the total CD spectrum near 190 nm. Because the couplet due to polarizability contributions is nearly symmetrical, the predicted CD spectrum is still conservative and therefore disagrees with experiment.

Following the results of *Madison* and *Schellman* [29] and *Tterlikkis et al.* [42], the *Ramachandran* ϕ and ψ angles were varied. As ϕ becomes less negative and ψ more positive, the couplet from polarizable groups becomes more asymmetric,

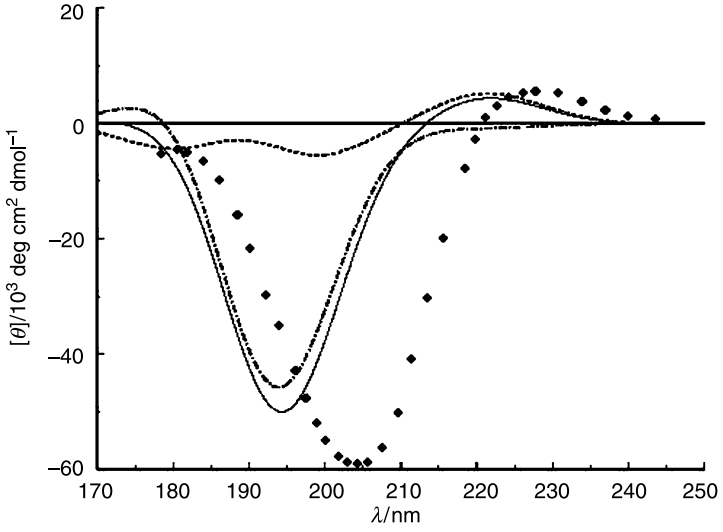

Fig. 9. CD spectra of a non-standard *PP*II helix ($-60°$, $+170°$) with N = 20 calculated using $\theta = -40°$; exciton contribution (- - - - - -); polarizable group contribution (- · · - · · -); total (———); the solid circles represent the experimental CD spectrum of *PP*II in water; see comment in caption for Fig. 8

with the negative lobe growing in intensity. However, the non-conservative character of the polarizable group contribution is never sufficient to fully overcome the strong positive couplet of the exciton contributions and a substantial positive band on the short-wavelength circle is predicted even for ($-60°$, $+180°$), the most extreme deviation considered (Fig. 8b).

The direction of the transition moment can also be varied. When $\theta = -40°$ was used, the exciton effect was found to be substantially weaker and the polarizable group contribution was strongly biased toward negative values. Figure 9 shows the results for ($-60°$, $+170°$). For this conformation, a strong negative band near 195 nm and only a very weak positive band near 170 nm are predicted. This set of parameters therefore reproduces the major features of the *PP*II CD spectrum quite well.

The effect of including polarizability contributions on the α-helix must be examined. The polarizability contributions also constitute a couplet for the α-helix, but the sign of this couplet changes between $\theta = -40°$ and $-55°$. For $-55°$, the couplet is positive, whereas it is negative for $\theta = -40°$. In both cases, the couplets are nearly symmetrical. However as shown in Fig. 10a, the positive polarizability couplet for $\theta = -55°$ weakens the 205 nm negative band and degrades agreement with experiment relative to the exciton-only prediction. Figure 10b shows the results for $\theta = -40°$. The negative lobe of the polarizability couplet combines with the weaker negative CD in the 205 nm region of the exciton calculation to produce a 205 nm band that is stronger than the 220 nm band. Thus the conclusion that *Clark*'s experimental transition moment direction for a secondary amide ($-55°$) is also optimal for reproducing the α-helix CD spectrum needs to be modified when polarizable groups are included. A value of $-40°$ to $-45°$ appears to be more suitable.

The direction of the NV_1 transition dipole moment depends on the electrostatic environment as well as on the nature of the amide (primary, secondary, tertiary). Local electrostatic potentials and fields can shift the transition energies and can

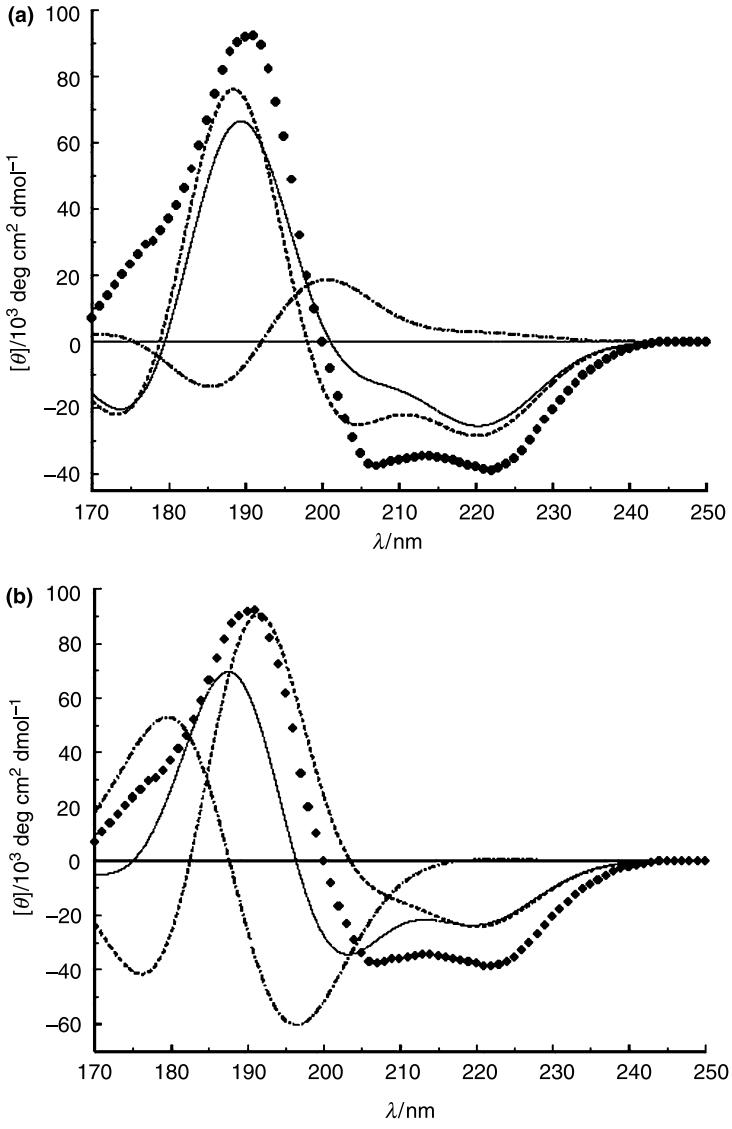

Fig. 10. CD spectra calculated for an α-helix with N = 20; exciton contribution (- - - - - -); polarizable group contribution (- · - · - · -); total (———); (a) $\theta = -55°$, (b) $\theta = -40°$

mix the NV_1 and NV_2 transitions, leading to rotation of both the NV_1 and NV_2 transition dipole moments. These effects have been calculated [45] for the amide crystals studied experimentally by *Clark* [28]. The methods used in the present work need to be extended to include the methods used in Ref. [45] so that the NV_1 transition moment is not treated as a fixed parameter in the calculation but is determined by the geometric and electronic structure of the polypeptide.

Finally, the effects of including polarizable group contributions provide a qualitative explanation of the discrepancies between predicted helix band intensities and those derived from experiment. For $\theta = -40°$, in both the α- and *PP*II-helix, the polarizable group contributions lead to couplets that are opposite in sign to the exciton helix band. This accounts for the over-prediction of helix band intensity by

exciton theory and for the failure to observe the short-wavelength exciton lobe predicted for the α- and *PP*II-helix.

In summary, exciton theory provides an excellent starting point for the description of the CD spectra of regular polypeptide secondary structures such as helices and β-sheets. However, *Moffitt*'s theory has required some modifications beyond those arising from the helix band [15]. First, the incorporation of the $n\pi^*$ transition required consideration of intrinsic magnetic dipole transition moments and of electrically forbidden transitions. This was accomplished by the first-order perturbation theory of *Tinoco* [46] and by the all-order matrix method of *Bayley et al.* [27].

Second, end effects in finite helices were studied by explicit calculation of the exciton eigenvectors [26, 29] instead of the use of analytical exciton coefficients derived from periodic boundary conditions [1]. This led to the prediction of qualitatively different behavior for very short helices *vis-á-vis* long helices. However, this result depends on the transition moment direction [31] and on whether mixing with high-energy transitions is included (present work).

Third, it is important to include mixing of the well-characterized transitions at accessible wavelengths with very high-energy transitions modeled by polarizabilities. The contributions of such mixing are critical in the case of *PP*II helices that show strongly non-conservative CD spectra in the accessible wavelength range. For systems exhibiting nearly conservative CD spectra, *e.g.*, α-helix and β-sheets, mixing with high-energy transitions does not alter the spectra in a major way, but it can lead to significant changes in the predicted spectra.

Methods

Prediction of the CD spectrum of a peptide requires the calculation of the rotational strengths for the electronic transitions of the amide groups in the peptide. Three discrete transitions in each amide are considered: the $n\pi^*$ transition at 220 nm, the first $\pi\pi^*$ transition (NV_1) at 190 nm, and the second $\pi\pi^*$ transition (NV_2) at 139 nm. The 3N rotational strengths (N is the number of amide groups) are calculated in two steps. First, the matrix method [27] in its origin-independent form [47] is used to calculate the mixing of the 3N discrete transitions amongst themselves. Calculations of this type have been performed for many peptides and proteins and have been reviewed recently [48, 49]. The parameters of *Woody* and *Sreerama* [50] are used in the present calculation, except for those calculations in which the NV_1 transition moment direction was the variable. The Hamiltonian, wave functions, and the electric and magnetic dipole transition moments are given by Eqs. (1)–(5). As an illustration, the perturbation matrix **V** for two identical groups with two excited states a and b is given by Eq. (18) where the E_{1a} *etc*. are the energies of the excited states in the isolated chromophores; V_{1a2b} represents the coupling energy of the transition densities 0→a in group 1 with that for 0→b in group 2; and V_{1a1b} represents the interaction of the transition densities a→b in group 1 with the permanent charge density of group 2. Diagonalization of the **V** matrix leads to the polymer excited-state energies E_k as the eigenvalues and the coefficients C_{jak} for Eqs. (3)–(5) as the eigenfunctions.

$$\mathbf{V} = \begin{pmatrix} E_{1a} & V_{1a1b} & V_{1a2a} & V_{1a2b} \\ V_{1a1b} & E_{1b} & V_{1b2a} & V_{1b2b} \\ V_{1a2a} & V_{1b2a} & E_{2a} & V_{2a2b} \\ V_{1a2b} & V_{1b2b} & V_{2a2b} & E_{2b} \end{pmatrix} \tag{18}$$

The wave function for excited state K($K = 1, \ldots, 3N$), Ψ_K is given by Eq. (19) in which ψ_{ia} is the wave function for the peptide with group *i* in excited state a and all other groups in their ground state.

The coefficient C_{iaK} is the element of the Kth eigenvector corresponding to ψ_{ia}, and its square specifies the extent to which ψ_{ia} contributes to the eigenvector. The rotational strength of the transition to excited state K is given by Eq. (20) [27, 47] where $\gamma = e^2\hbar^2/4\pi m^2c^2$; λ_K is the wavelength of the transition to excited state K; ∇_{i0a} is the matrix element of the gradient operator for transition 0→a in group i; and $(\mathbf{r}\times\nabla)_{j0b}$ is the matrix element of the $(\mathbf{r}\times\nabla)$ operator for transition 0→b in group j. The summations are over all N groups and all three locally excited states.

$$\Psi_K = \Sigma C_{iaK}\,\psi_{ia} \tag{19}$$

$$R_K = \gamma\lambda_K\nabla_{0K}\bullet(\mathbf{r}\times\nabla)_{0K} = \gamma\lambda_K\Sigma_i\Sigma_a\Sigma_j\Sigma_b C_{iaK}C_{jbK}\nabla_{i0a}\bullet(\mathbf{r}\times\nabla)_{j0b} \tag{20}$$

The gradient matrix element is related to the electric dipole transition moment in the length representation by the *Heisenberg* equation of motion (Eq. (21)) [51]

$$\nabla_{i0a} = (2\pi mc/e\hbar)\boldsymbol{\mu}_{i0a}/\lambda_{0a} \tag{21}$$

Thus ∇_{i0a} is zero for the electrically forbidden $n\pi^*$ transition and can be calculated from the electric dipole transition moments for the electrically allowed NV_1 and NV_2 transitions. The matrix element $(\mathbf{r}\times\nabla)_{j0b}$ depends on the choice of origin and is given by Eq. (22) where $\mathbf{r}'$ is the position vector relative to a local origin centered on the chromophore, and $\mathbf{R}_j$ is the position vector of this local origin in the molecular coordinate system (note that although the matrix element in Eq. (22) depends on the origin, the rotational strengths from Eq. (20) do not). The first term on the right-hand side of Eq. (22) is related to the intrinsic magnetic dipole transition moment. For the $n\pi^*$ transition, this is the only non-zero contribution because $\nabla_{n\pi^*} = 0$. For the NV_1 and NV_2 transitions, we locate the origin of the local coordinate system at the amide carbonyl carbon [52] and neglect the intrinsic contribution, $(\mathbf{r}'\times\nabla)_{j0b}$.

$$(\mathbf{r}\times\nabla)_{j0b} = (\mathbf{r}'\times\nabla)_{j0b} + \mathbf{R}_j\times\nabla_{j0b} \tag{22}$$

In the second stage of the calculations, the excited states described in Eq. (19) are allowed to mix with high-energy transitions in the peptide backbone and in the side chains. Their contribution to the rotational strengths of the discrete transitions can be described by perturbation theory, following methods developed by *Tinoco* and co-workers [23, 46] and by *Zubkov* and *Vol'kenshtein* [53]. Early calculations of peptide CD included the effects of high-energy transitions *via* polarizable groups [23, 40, 41, 53]. However, the method requires information about polarizability tensors of groups rather than simply the mean polarizability. Accurate experimental data on the polarizability tensors of amides and other relevant groups are lacking even now. The tensor parameters used in the early calculations were highly uncertain. For example, the amide group has been approximated by an ellipsoid with a symmetry axis normal to the plane and a negative anisotropy [23] and by an ellipsoid with positive anisotropy and the symmetry axis approximately along the carbonyl bond [54], based on the dipole interaction model [55]. Because of these uncertainties, the practice of including contributions from the high-energy transitions fell out of fashion. That these contributions are likely to be important, especially for *PP*II, is suggested by the failure of the matrix method calculations that included only the known amide transitions and the success of *Applequist*'s classical polarizability or dipole interaction model [56, 57].

Ab initio methods are now available for calculating accurate molecular polarizabilities. Using localized *ab intio* wave functions and finite-field perturbation methods, *Garmer* and *Stevens* [58] reported polarizability tensors for bonds and lone-pairs in a number of molecules. In the present work, bond and lone-pair polarizability tensors derived for *N*-methylacetamide by *W. Stevens* (private communication) are used. Following the methods of *Tinoco* [46], the contribution of the high-energy transitions to the rotational strength of the transition 0→K is given by Eq. (23) where $f(\lambda_K) = \pi\lambda_K/(\lambda_K{}^2 - \lambda_0{}^2)$ and λ_0 is the average wavelength of the high-energy transitions, assumed to be 100 nm; q_{jbt} is a point charge located at the position $\mathbf{R}_{jbt}$ such that $\Sigma_t\, q_{jbt}\,\mathbf{R}_{jbt} = \boldsymbol{\mu}_{j0b}$, that is the electric dipole transition moment $\boldsymbol{\mu}_{j0b}$ is treated in the monopole or distributed dipole approximation; the vector from monopole t of transition 0→b on group j to polarizable group l is $\mathbf{R}_{jbt,l} = \mathbf{R}_l - \mathbf{R}_{jbt}$, and $|\mathbf{R}_{jbt,l}|$ is the length of this vector; the polarizability tensor of group l is α_l; and the vector from

group i to polarizable group l is $\mathbf{R}_{il} = \mathbf{R}_l - \mathbf{R}_i$. Details of the method and the polarizability parameters will be described elsewhere (*Woody*, to be published).

$$R_{K\alpha} = f(\lambda_K)\Sigma_i\Sigma_a\Sigma_j\Sigma_b\Sigma_{l\neq j}\Sigma_t C_{iaK}C_{jbK}\{q_{jbt}\mathbf{R}_{jbt,l} \bullet \alpha_l \bullet \boldsymbol{\mu}_{ia} \times \mathbf{R}_{il}/|\mathbf{R}_{jbt,l}|^3\} \tag{23}$$

CD spectra are calculated from the theoretical wavelengths λ_K and the rotational strengths R_K, including both types of contributions, assuming *Gaussian* band shapes, as shown in Eq. (24) where $[\theta^0]_K$ is the amplitude of the Kth CD band (Eq. (25)); N_0 is *Avogadro's* number; h is *Planck's* constant; c is the velocity of light; μ_B is the *Bohr* magneton; R_K(cgs) is the rotational strength of the Kth transition in cgs units; and R_K(*DB*M) is the rotational strength in units of *Debye-Bohr* magnetons (1 *DB*M $= 10^{-18}\mu_B$ cgs units). The bandwidth for the transition 0→K, Δ_K, is calculated as the weighted average of the bandwidths for the monomer transitions, $\Delta_{ia,}$ (Eq. (26)).

$$[\theta](\lambda) = \Sigma_K[\theta^0]_K \exp[-(\lambda - \lambda_K)^2/{\Delta_K}^2] \tag{24}$$

$$\begin{aligned}[\theta^0]_K &= (48\pi^{3/2}N_0/hc)[R_K(cgs)]\lambda_K/\Delta_K \\ &= (48\pi^{3/2}N_0/hc)[10^{-18}\mu_B R_K(DBM)]\lambda_K/\Delta_K \\ &= 7515R_K(DBM)\lambda_K/\Delta_K\end{aligned} \tag{25}$$

$$\Delta_K = \Sigma_i\,\Sigma_a\,{C_{iaK}}^2\,\Delta_{ia} \tag{26}$$

These bandwidths were taken to be [50] 10.5, 11.3, and 7.2 nm for the $n\pi^*$, NV_1, and NV_2 transitions.

Acknowledgements

The author is grateful to Dr. *W. J. Stevens*, Center for Advanced Research in Biotechnology, Gaithersburg MD, for providing the polarizability tensors of *N*-methylacetamide. The assistance of Ms. *K. Harding* and Dr. *N. Sreerama* in manuscript preparation is gratefully acknowledged. This work was supported by NIH grant EB002803.

References

[1] Moffitt W (1956) J Chem Phys **25**: 467
[2] Moffitt W (1956) Proc Natl Acad Sci USA **42**: 736
[3] Pauling L, Corey RB, Branson HR (1951) Proc Natl Acad Sci USA **37**: 205
[4] Peterson DL, Simpson WT (1955) J Am Chem Soc **77**: 3929
[5] Peterson DL, Simpson WT (1957) J Am Chem Soc **79**: 2375
[6] Moffitt W, Yang JT (1956) Proc Natl Acad Sci USA **42**: 596
[7] Rosenheck K, Doty P (1961) Proc Natl Acad Sci USA **47**: 1775
[8] Tinoco I, Halpern A, Simpson WT (1962) The relation between conformation and light absorption in polypeptides and proteins. In: Stahman MA (ed) Polyamino Acids, Polypeptides, and Proteins. University of Wisconsin Press, Madison, p 147
[9] Gratzer WB, Holzwarth GM, Doty P (1961) Proc Natl Acad Sci USA **47**: 1785
[10] Mandel R, Holzwarth G (1972) J Chem Phys **57**: 3469
[11] Holzwarth G, Gratzer WB, Doty P (1962) J Am Chem Soc **84**: 3194
[12] Brahms J, Spach G (1963) Nature **200**: 72
[13] Toumadje A, Alcorn SW, Johnson WC Jr (1992) Anal Biochem **200**: 321
[14] Jenness DD, Sprecher C, Johnson WC Jr (1976) Biopolymers **15**: 513
[15] Moffitt W, Fitts DD, Kirkwood JG (1957) Proc Natl Acad Sci USA **43**: 723
[16] Ando T (1968) Progr Theor Phys **40**: 471
[17] Loxsom FM (1969) J Chem Phys **51**: 4899
[18] Deutsche CW (1970) J Chem Phys **52**: 3703

[19] Rosenfeld L (1928) Z Phys **52**: 161
[20] Tinoco I Jr (1964) J Am Chem Soc **86**: 297
[21] Mason SF (1963) Quart Rev (London) **17**: 20
[22] Holzwarth G, Doty P (1965) J Am Chem Soc **87**: 218
[23] Woody RW, Tinoco I Jr (1967) J Chem Phys **46**: 4927
[24] Cassim JY, Yang JT (1970) Biopolymers **9**: 1475
[25] Johnson WC Jr, Tinoco I Jr (1972) J Am Chem Soc **94**: 4389
[26] Tinoco I Jr, Woody RW, Bradley DF (1963) J Chem Phys **38**: 1317
[27] Bayley PM, Nielsen EB, Schellman JA (1969) J Phys Chem **73**: 228
[28] Clark LB (1995) J Am Chem Soc **117**: 7974
[29] Madison V, Schellman J (1972) Biopolymers **11**: 1041
[30] Siedlicka M, Goch G, Ejchart A, Sticht H, Bierzynski A (1999) Proc Natl Acad Sci USA **96**: 903
[31] Chin D-H, Woody RW, Rohl CA, Baldwin RL (2002) Proc Natl Acad Sci USA **99**: 15416
[32] Adzhubei AA, Eisenmenger F, Tumanyan VG, Zinke M, Brodzinski S, Esipova NG (1987) Biochem Biophys Res Comun **146**: 934
[33] Adzhubei AA, Sternberg MJE (1993) J Mol Biol **229**: 472
[34] Sreerama N, Woody RW (1994) Biochemistry **33**: 10022
[35] Tiffany ML, Krimm S (1968) Biopolymers **6**: 1379
[36] Woody RW (1992) Adv Biophys Chem **2**: 37
[37] Shi Z, Woody RW, Kallenbach NR (2002) Adv Protein Chem **62**: 163
[38] Mandel R, Holzwarth G (1973) Biopolymers **12**: 655
[39] Cowan PM, McGavin S (1955) Nature **176**: 501
[40] Pysh ES (1967) J Mol Biol **23**: 587
[41] Ronish EW, Krimm S (1974) Biopolymers **13**: 1635
[42] Tterlikkis L, Loxsom FM, Rhodes W (1973) Biopolymers **12**: 675
[43] Manning MC, Woody RW (1991) Biopolymers **31**: 561
[44] Condon EU (1937) Rev Mod Phys **9**: 432
[45] Woody RW, Raabe G, Fleischhauer J (1999) J Phys Chem B **103**: 8984
[46] Tinoco I Jr (1962) Adv Chem Phys **4**: 113
[47] Goux WJ, Hooker TM Jr (1980) J Am Chem Soc **102**: 7080
[48] Hirst JD, Colella K, Gilbert ATB (2003) J Phys Chem B **107**: 11813
[49] Sreerama N, Woody RW (2004) Meth Enzymol **383**: 318
[50] Woody RW, Sreerama N (1999) J Chem Phys **111**: 2844
[51] Bohm D (1951) Quantum Theory. Prentice-Hall, Englewood Cliffs NJ, p 427
[52] Woody RW (1993) Tetrahedron Assymm **4**: 529
[53] Zubkov V, Vol'kenshtein MV (1970) Mol Biol (Eng Trans Molekul Biol) **4**: 483
[54] Blauer G, Sreerama N, Woody RW (1993) Biochemistry **32**: 6674
[55] Applequist J, Carl JR, Fung K-K (1972) J Am Chem Soc **94**: 2952
[56] Applequist J (1981) Biopolymers **20**: 2311
[57] Bode KA, Applequist J (1996) J Phys Chem **100**: 17825
[58] Garmer DR, Stevens WJ (1989) J Phys Chem **93**: 8263